Rapid prototyping for fabrication of GHz-THz bandgap structures

Michael E. Gehm[a,b], Ziran Wu[c], and Hao Xin[a,c]

[a]Department of Electrical and Computer Engineering, University of Arizona, Tucson, AZ;
[b]College of Optical Sciences, University of Arizona, Tucson, AZ;
[c]Department of Physics, University of Arizona, Tucson, AZ

ABSTRACT

Recent advances in rapid prototyping technologies have resulted in build-resolutions that are now on the scales required for direct fabrication of photonic structures in the gigahertz (GHz) and terahertz (THz) regimes. To demonstrate this capability, we have fabricated several structures with 3D bandgaps in these spectral regions. Characterization of the transmission properties of these structures confirms the build accuracy of this fabrication method. The result is a rapid and inexpensive fabrication technique that can be utilized to create a variety of interesting photonic structures in the GHz and THz. We present the results of our characterization experiments and discuss our current efforts in extending the technique to fabrication of other structure types.

Keywords: photonic bandgap materials, electromagnetic bandgap materials, photonic crystals, gigahertz components, terahertz components, fabrication technologies

1. INTRODUCTION

Electromagnetic bandgap (EBG) materials are among the most rapidly-evolving subfields of applied electromagnetic research. The ability to control the propagation-mode density-of-states in these materials can provide revolutionary capabilities in almost all areas of applied electromagnetics (emission,[1] detection,[2] filtering,[3] guiding,[4] etc.)—hence the great interest and rapid progress in the field.

Further, the GHz and THz spectral bands—long-neglected compared to their microwave and infrared/optical neighbors—have also emerged as a central features of modern electromagnetic research. The growing attention on these spectral bands is the inevitable result of continuing progress in communications and sensing. In communications, the need for ever-increasing bandwidth is moving applications that have historically resided deep in the RF and microwave bands upward in frequency towards and into the GHz and THz. Simultaneously, the security-screening needs of the modern world are driving a search for non-ionizing sensing capabilities that can quickly and easily scan for concealed items. The desire to combine reasonable spatial localizability with safe, penetrative capability necessitates the use of GHz and THz frequencies.

As a result, progress in these spectral bands is currently undergoing something of a renaissance; with burgeoning applications in contraband detection,[5,6] tumor recognition and imaging,[7,8] DNA analysis,[9,10] radar,[11,12] and communication.[13,14] A significant challenge remains, however—component fabrication. The feature dimensions of GHz and THz components fall in a transition region between the conventional micromachining techniques used for microwave applications, and the various micro-/nanofabrication methods developed for use at optical wavelengths. A number of semiconductor fabrication approaches, including dicing-saws,[15] wet etching,[16] deep reactive ion etching (DRIE),[17] deep x-ray lithography,[18] and laser micromachining[19] have been repurposed for fabrication in these spectral bands. These methods remain very expensive, however, and require significant care to achieve THz-scale features of reasonable uniformity. Further, many of these approaches have limited applicability for the complicated 3D structures now routinely being considered.

Advances in rapid-prototyping technologies have resulted in build-resolutions that fall within the desired length-scale range. As a result, direct fabrication of GHz-THz photonic structures has become possible on these machines. We have recently utilized this approach to fabricate a variety of structures with bandgaps and

Corresponding address: gehm@ece.arizona.edu

Terahertz Physics, Devices, and Systems III: Advanced Applications in Industry and Defense
edited by Mehdi Anwar, Nibir K. Dhar, Thomas W. Crowe, Proc. of SPIE Vol. 7311
73110F · © 2009 SPIE · CCC code: 0277-786X/09/$18 · doi: 10.1117/12.818397

other interesting properties in the 100–400 GHz range. Experimental measurements show excellent agreement with simulation, thereby demonstrating the build accuracy of this approach. Fabrication using this approach is extremely rapid and inexpensive, resulting in wide applicability to future THz applications.

2. FABRICATION METHODOLOGY

EBG-physics is fundamentally a multiple-scattering phenomenon. As such, the structures require feature sizes on the scale of the wavelength or below. For our frequency range of interest (100 GHz–10 THz), the corresponding wavelength range is 3 mm–30 μm. The specific relationship between band location and feature size is, of course, highly dependent on the details of the particular structure. As a practical matter, however, we might take the range 1 mm-10 μm as a reasonable estimate of the required feature scale.

Polymer-jetting is an additive rapid prototyping (RP) technique that now has build resolutions that fall within this range. The lab of one of the authors (MG) contains a commercial rapid prototyping machine (Objet Eden 350) that claims a fundamental resolution of 42 μm in the x and y directions and 16 μm in z. Fabrication within the RP machine occurs on top of a tray that can be lowered in 16 μm increments. The heart of the machine is a set of print heads (analogous to those on an inkjet printer) that deposits a 16 μm-thick layer of polymer on the tray and cures it using ultraviolet lamps. The tray is then lowered and the next slice of the object is printed on top of the previously printed slice. In this manner, the desired object is assembled sequentially out of a large number of 16 μm slices.

In general, very few slices of the physical object would be fully supported by the slice below. To counteract this problem, the RP machine makes use of two materials—a *model* material which forms the structure of the desired part, and a *support* material which is deposited where necessary to provide a suitable foundation for later slices. After the entire model is complete, the construction tray rises and the part may be removed. For traditional rapid prototyping tasks, the finishing step involves using a high-pressure water spray to remove the gelatin-like support material, leaving just the model material in the desired 3D shape.

Initial attempts at constructing our desired EBG structures via this technique revealed several areas where we needed to modify this approach, or adapt certain constraints on our desired structures. First, the model structure is a collection of fused polymer droplets. Despite the stated resolution of the machine (42 μm $\times$ 42 μm $\times$ 16 μm), the globular nature of the resulting part lacks physical cohesion for features smaller than $\approx 200\mu$m in x and y. Thus we limit our designs to those scales. As this is a factor of 20 larger than the minimum desired feature size (10 μm), we expect the maximum frequency to scale inversely by a similar factor. Thus with this spatial resolution, we might expect bandgaps at frequencies up to ≈ 500 GHz.

A second challenge is that even at this resolution, the resulting structures are often too fragile to survive significant washing with the high-pressure water spray. Alternating periods of soaking in a 3% aqueous solution of NaOH and gentle washing in water eventually loosens and removes the support material. Finally, any method for support material removal requires *access* to the support material. Thus, our designs must either incorporate such access channels, or must utilize encapsulated support material as an alternative dielectric in the design.

Construction of THz EBG structures with this system is both rapid and inexpensive. Clearly the fabrication time is dependent on the volume of the component. However, for the parts discussed in this manuscript, the fabrication times have been on the order of 30 minutes. The associate consumable costs have also been quite low, approximately $10 per part.

3. EXPERIMENTAL DEMONSTRATION

To demonstrate the value of the polymer-jetting RP technique, we designed and fabricated several EBG structures and experimentally measured their properties using a THz time-domain spectrometer (THz-TDS) that is available to one of the authors (HX). A THz-TDS operates by sending a picosecond pulse through the component under test. The short time domain implies a broad bandwidth, and the resulting time-domain transmission signal can be Fourier transformed to extract the frequency content of the pulse after interaction with the component. By comparing this with the free-space result, the frequency-dependent transmission properties of the component can be determined. The particular instrument has a spectral range of 50 GHz–1.2 THz and a maximum frequency

resolution of 0.417 GHz. The results of the measurements and their comparison with simulation are discussed below.

3.1 CHARACTERIZATION OF POLYMER MATERIAL

For the design (and eventual simulation) of the structures, it was first necessary to characterize the electromagnetic properties of the model polymer, specifically the complex permittivity ($\epsilon = \epsilon' - j\epsilon''$) and permeability ($\mu = \mu' - j\mu''$). As the polymer is non-magnetic ($\mu = 1$), the complex permittivity can be determined by performing a single transmission measurement using the THz-TDS. The dielectric constant ϵ' and the loss tangent $\tan\delta = \epsilon''/\epsilon'$ of the material can then be extracted from the magnitude and phase of the transmission coefficient. Characterization of the model material was performed on a 3 mm thick slab of the material. Characterization of the support material was performed by measuring a 1 mm thick layer of support material encapsulated between two 1 mm thick walls of model material. The dielectric constant and loss tangent for the model material are plotted in Fig. 1. A slow decrease of the dielectric constant is observed as frequency increases, from 2.78 at 100 GHz to 2.7 at 600 GHz. The material loss tangent slowly increases from 0.02 around 100 GHz to 0.05 at 600 GHz.

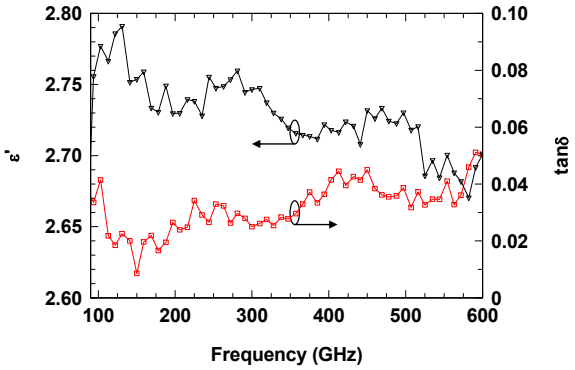

Figure 1. Polymer slab THz characterization results. The real part of the permittivity ϵ' (open triangles) is plotted with the left ordinate, and the loss tangent $\tan\delta$ (open squares) is plotted with the right ordinate.

From these results, we can determine that the model material has a refractive index ($n = \mathrm{Re}[\sqrt{\epsilon}]$) of approximately 1.66 in our desired spectral range. Our desired structures will use air ($n \approx 1$) as the contrasting dielectric. This provides sufficient index contrast for periodic structures to produce bandgaps, although the bandgaps will not be as wide as in systems with larger contrast. We are currently investigating methods for increasing the index of the model material in order to allow greater contrast.

3.2 WOODPILE STRUCTURE

Our initial test was performed with the familiar woodpile structure (WPS),[20] which is known to have a complete 3D bandgap. A schematic of this structure is shown in Fig. 2(a) (from[21]). The structure is based upon a unit cell of thickness D built from four layers of long rods (rectangular in cross-section and with alternating orientations between layers). Within each layer, the rods are spaced with periodicity d, and adjacent layers with the same orientation are shifted with respect to each other by $d/2$. Each rod has a height $h = D/4$ and a width $w = h$. The resulting filling ratio is therefore equal to w/d. The structure is a face-centered-tetragonal (fct) lattice (see Fig. 2(a)). The center frequency and width of the WPS bandgap can be scaled by adjusting the structure parameters.

Using the previously measured index of refraction, we were able to design a woodpile structure with a predicted bandgap at 185 GHz. Figure 2(b) shows a photograph of the fabricated part. The WPS parameters were $w = h = 352$ μm with a periodicity $d = 1292$ μm. There were 5 unit cells in the stacking direction and the transverse size was sufficient to fully block the THz-TDS beam. The inset of Fig. 2(b) is an enlarged view of the sample cross-section showing clean, sharp features with the desired geometric structure.

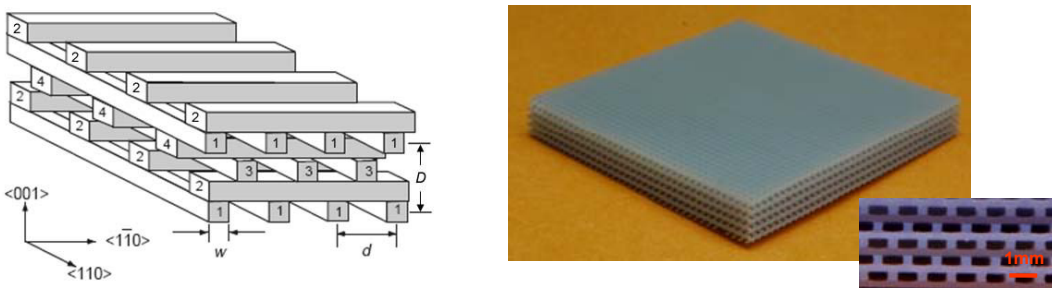

(a) (b)

Figure 2. (a) A schematic drawing of the woodpile structure (from[21]). (b) Photographs of the fabricated polymer THz WPS. Inset is an enlarged view of the sample cross-section.

We then measured the transmission of the WPS using the THz-TDS. The WPS was oriented so that the pulse was incident along the stacking direction. The resulting power transmission spectrum is shown in Fig. 3 (open squares). We see that the fabricated structure has a fundamental bandgap near 180 GHz with a band rejection greater than 35 dB. Secondary and tertiary bandgaps are also visible. If we use a 15 dB change from the band center as the definition of the band edges, the primary bandgap has a width of $\approx$ 48 Ghz. The bandwidth to center frequency ratio $\Delta f/f_c$ is therefore approximately 27%, qualifying the structure as a good notch filter.

The experimental results were then compared to a full-wave finite-element simulation performed in HFSS. For the simulation, we modeled the polymer as a pure dielectric with $\epsilon' = 2.76$ and $\tan\delta = 0.06$. The loss tangent was chosen to be slightly higher than the maximum observed value so that the simulation did not underestimate material loss. The result of the simulation is shown in Fig. 3 (solid line). Excellent agreement is observed between the experimental and simulation results. In addition to clear correspondence in the primary, secondary, and tertiary bandgaps, the simulation and experiment also both reveal a small resonance feature near 202 GHz. The overall quality of the match confirms the fabrication accuracy of the polymer-jetting RP approach.

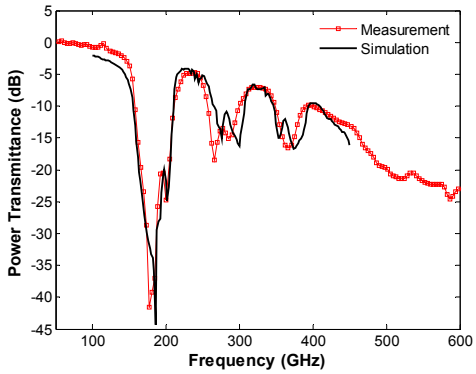

Figure 3. Comparison between the measured (open squares) and simulated (solid line) WPS normal-incidence power transmittances.

3.3 "JOHNSON" STRUCTURE

For our second test, we utilized a more complicated EBG structure first proposed by Johnson and Joannopoulos,[22] and later fabricated by the same group.[23] We refer to this as the "Johnson-structure" (JS). The JS consists of two alternating 2D triangular lattice layers, one being an array of pseudohexagonal dielectric rods (the "rod layer") and the other being an array of holes in a dielectric sheet (the "hole layer"). The holes have a radius r

and the pillar size is defined as by the radii of the adjacent holes in the neighboring layers. The rod and hole layers have a common lattice constant x, and subsequent layers are shifted by $x/\sqrt{3}$ in the x direction.

For our EBG structure, we took the dimensions of the original structure (designed for the optical bands) and scaled them to the GHz/THz region. Specifically, our JS has the following dimensions: lattice constant $x = 1346$ μm, hole radius $r = 500$ μm, dielectric sheet thickness $h = 1713$ μm, and rod height $t = 1071$ μm. There were three unit cells in the stacking direction (9 hole layers and 9 rod layers). Based on these parameters, the structure was expected to exhibit a complete bandgap around 200 GHz.

The fabricated JS is shown in Fig. 4(left). Enlarged views of the side and top of the structure are shown in Fig. 4(right), clearly showing the inter-layer shifting and the hole array. Again, the features are clean and sharp, and demonstrate the required geometric structure.

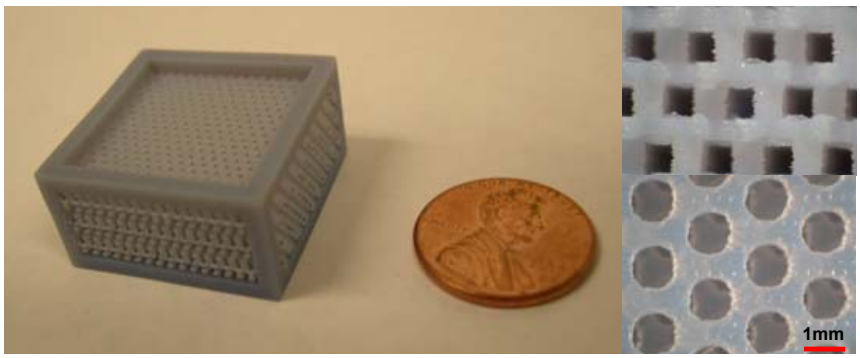

Figure 4. Photographs of the fabricated polymer Johnson EBG structure, including: the full view (left), the side (cross-sectional) view (upper right), and the top view (lower right). Clearly defined air hole and dielectric rod layers are observed.

As with the WPS, we used the THz-TDS to measure the transmission of the JS. The measured power transmission spectrum is shown in Fig. 5. As the JS component was thicker than the WPS component, a larger amount of loss was observed. As a result, the noise-floor of the THz-TDS becomes significant for frequencies above 350 GHz. Therefore we limit our analysis to the range 50–350 GHz. A fundamental bandgap exists at ≈ 223 GHz, with a band rejection of ≈ 25 dB. The ratio of bandwidth to center frequency $\Delta f/f_c$ for this feature is approximately 15%—somewhat less effective than the WPS. A secondary transmission dip is also seen near 117 GHz, with a band rejection of approximately 15 dB.

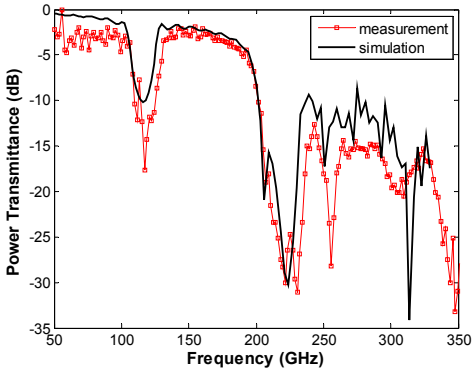

Figure 5. Comparison between the measured (open squares) and simulated (solid line) Johnson structure normal-incidence power transmittances.

We then performed a full electromagnetic simulation of the JS using HFSS. The results are plotted as the solid curve in Fig. 5. There is good general agreement on the location, width, and depth of the fundamental bandgap near 225 GHz as well as the secondary feature near 120 GHz. Other features seen in the measurement, such as those at 255 and 309 GHz, also resemble features in the simulation, but the approach of the noise-floor reduces the significance of the match. Once again, the results confirm the overall capability of the polymer-jetting RP approach.

4. EXTENSION TO BRAGG-SELECTIVE DIFFRACTIVE OPTICS (VOLUME HOLOGRAMS)

The bandgap properties of EBG structures arise from the Bloch solutions that result from the periodic (or nearly-periodic) physical configuration of the component. If we relax the requirement of periodicity, the bandgaps disappear, but the structure remains a general *diffractive optic*—with a number of useful performance features over traditional refractive components.

Clearly the polymer-jetting RP approach can also be used to fabricate structures of this type. As with EBG structures, it is easy to design complicated 3D diffractive optics, but fabrication can remain a challenge in all but the simplest of cases. As a result, a number of strategies for diffractive optic design are founded on layer-based approaches that are most easily matched to fabrication technology. A more general approach (but one that requires arbitrary 3D fabrication technology) is to consider the *Bragg scattering* domain, in which both the incoming field and the optic are decomposed in a plane-wave basis to yield their corresponding *wavevector spectra*. The wavevector spectrum of the outgoing field is then all possible vector sums of an incoming wavevector and an optic wavevector (conserves photon momentum), that also satisfy $k_{\text{out}}^2 = k_{\text{in}}^2 + k_{\text{optic}}^2$ (conserves photon momentum).

In this regime, the optic is said to be *Bragg-selective*, as only certain direction/wavelength combinations will satisfy these constraints and be scattered by the optic. Structures with the property are also referred to as *volume holograms*. It then becomes possible to design Bragg-selective optics by taking the desired output wavevector spectrum and the known input wavevector spectrum, and solving for the wavevector spectrum that best couples the input and output states. The result will be the wavevector spectrum of the desired optic, and the inverse 3D Fourier transform of this spectrum yields the 3D spatial variation of refractive index of the desired device

$$n(x, y, z) \propto \mathcal{F}^{-1}[\vec{k}_{\text{opt}}(f_x, f_y, f_z)]. \tag{1}$$

The resulting $n(x, y, z)$ can be normalized to fall in the range available to the fabrication technique, but the result will still be a continuous variation of n within this range. Given the current polymer-jetting RP technique, we are limited to two discrete index values (model/support or model/air). However, we can make use of *effective-medium theory* to achieve the effect of continuous index variation. The desired index profile $n(x, y, z)$ is first spatially discretized on a scale that is on the order of the wavelength λ and the average value of n is computed in each of these regions. Then, the spatial regions are further divided into spatial cells of size much less than λ. The cells within a λ^3 region are then randomly apportioned between the two materials in a proportion that achieves the desired average value of n within that λ^3 region.

We have begun investigating the use of this technique to fabricate THz volume holograms. Figure 6 shows one quadrant of the structure we are currently designing. Note the complicated 3D structure that would be extremely difficult (or impossible) to fabricate by other means. We are currently validating the design via HFSS calculations and hope to fabricate and experimentally test the structure in the near future.

5. SUMMARY

We have successfully used polymer-jetting RP to fabricate high-quality 3D EBG structures in the GHz and THz bands. Experimental measurements of the structures demonstrate extremely good correspondence with simulation, confirming the high dimensional accuracy and geometric complexity achievable with this technique. The great advantages of the additive RP approach are that 1) it enables fabrication of a broad class of arbitrary 3D structures and 2) fabrication time and cost are minimal and largely independent of structure complexity.

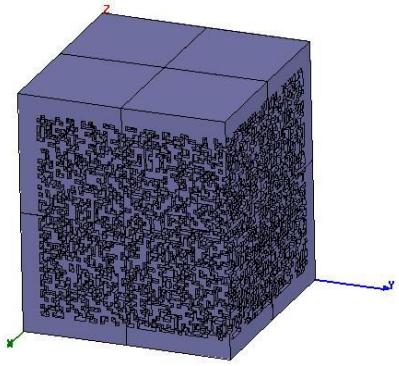

Figure 6. One spatial quadrant of the THz volume hologram currently under design for eventual fabrication via polymer-jetting RP.

These features make the technique highly promising for further EBG applications. Further, the general technique should also be applicable to fabrication of less-specialized components in the GHz/THz bands. We are currently investigating Bragg-selective structures such as volume holograms and expect to soon fabricate and test our first designs.

REFERENCES

[1] Lodahl, P., Van Driel, A., Nikolaev, I., Irman, A., Overgaag, K., Vanmaekelbergh, D., and Vos, W., "Controlling the dynamics of spontaneous emission from quantum dots by photonic crystals," *Nature* **430**, 654–657 (2004).

[2] De Maagt, P., Gonzalo, R., Vardaxoglou, Y., and Baracco, J., "Electromagnetic bandgap antennas and components for microwave and (sub) millimeter wave applications," *IEEE Transactions on Antennas and Propagation* **51**(10 Part 1), 2667–2677 (2003).

[3] Kim, T. and Seo, C., "A novel photonic bandgap structure for low-pass filter of widestopband," *IEEE Microwave and Guided Wave Letters* **10**(1), 13–15 (2000).

[4] Mekis, A., Chen, J., Kurland, I., Fan, S., Villeneuve, P., and Joannopoulos, J., "High transmission through sharp bends in photonic crystal waveguides," *Physical Review Letters* **77**(18), 3787–3790 (1996).

[5] Siegel, P., "Terahertz technology," *Microwave Theory and Techniques, IEEE Transactions on* **50**(3), 910–928 (2002).

[6] Kemp, M., Taday, P., Cole, B., Cluff, J., Fitzgerald, A., and Tribe, W., "Security applications of terahertz technology," in [*Proceedings of SPIE*], **5070**, 44, SPIE (2003).

[7] Löffler, T., Bauer, T., Siebert, K., Roskos, H., Fitzgerald, A., and Czasch, S., "Terahertz dark-field imaging of biomedical tissue," *Optics Express* **9**(12), 616–621 (2001).

[8] Woodward, R., Wallace, V., Pye, R., Cole, B., Arnone, D., Linfield, E., and Pepper, M., "Terahertz Pulse Imaging of ex vivo Basal Cell Carcinoma," *Journal of Investigative Dermatology* **120**(1), 72–78 (2003).

[9] Brucherseifer, M., Nagel, M., Bolivar, P., Kurz, H., Bosserhoff, A., and Büttner, R., "Label-free probing of the binding state of DNA by time-domain terahertz sensing," *Applied Physics Letters* **77**, 4049 (2000).

[10] Fischer, B., Walther, M., and Jepsen, P., "Far-infrared vibrational modes of DNA components studied by terahertz time-domain spectroscopy," *Physics in Medicine and Biology* **47**(21), 3807–3814 (2002).

[11] DeMartinis, G., Goyette, T., Coulombe, M., Waldman, J., and Nixon, W., [*A 1.56 THz Spot Scanning Radar Range for Fully Polarimetric W-Band Scale Model Measurements*], Defense Technical Information Center (2000).

[12] McMillan, R., [*Terahertz Imaging, Millimeter-Wave Radar*], Springer (2006).

[13] Mann, C., [*Towards Terahertz Communications Systems*], Kluwer Academic Publishers (2001).

[14] Rieh, J., Jagannathan, B., Greenberg, D., Meghelli, M., Rylyakov, A., Guarin, F., Yang, Z., Ahlgren, D., Freeman, G., Cottrell, P., et al., "SiGe heterojunction bipolar transistors and circuits toward terahertz communication applications," *Microwave Theory and Techniques, IEEE Transactions on* **52**(10), 2390–2408 (2004).

[15] Chelnokov, A., Rowson, S., Lourtioz, J., Duvillaret, L., and Coutaz, J., "Terahertz characterisation of mechanically machined 3D photoniccrystal," *Electronics Letters* **33**(23), 1981–1983 (1997).

[16] Baumann, F., Bailey, Jr, W., Naweed, A., Goodhue, W., and Gatesman, A., "Wet-etch optimization of free-standing terahertz frequency-selective structures," *Optics Letters* **28**(11), 938–940 (2003).

[17] Jukam, N. and Sherwin, M., "Two-dimensional terahertz photonic crystals fabricated by deep reactive ion etching in Si," *Applied Physics Letters* **83**, 21 (2003).

[18] Feiertag, G., Ehrfeld, W., Freimuth, H., Kolle, H., Lehr, H., Schmidt, M., Sigalas, M., Soukoulis, C., Kiriakidis, G., Pedersen, T., et al., "Fabrication of photonic crystals by deep x-ray lithography," *Applied Physics Letters* **71**, 1441 (1997).

[19] Walker, C., Narayanan, G., Knoepfle, H., Capara, J., Glenn, J., Hungerford, A., Bloomstein, T., Palmacci, S., Stern, M., and Curtin, J., "Laser Micromachining of Silicon: A New Technique for Fabricating High Quality Terahertz Waveguide Components," in [*Proc. Eighth International Symposium on Space Terahertz Technology*], 358–376 (1997).

[20] Ho, K., Chan, C., Soukoulis, C., Biswas, R., and Sigalas, M., "Photonic band gaps in three dimensions: new layer-by-layer periodic structures," *Solid State Communications* **89**(5), 413–416 (1994).

[21] Lin, S., Fleming, J., Hetherington, D., Smith, B., Biswas, R., Ho, K., Sigalas, M., Zubrzycki, W., Kurtz, S., and Bur, J., "Athree-dimensional photonic crystal operating at infraredwavelengths," *Nature* **394**, 251 (1998).

[22] Johnson, S. and Joannopoulos, J., "Three-dimensionally periodic dielectric layered structure with omnidirectional photonic band gap," *Applied Physics Letters* **77**, 3490 (2000).

[23] Qi, M., Lidorikis, E., Rakich, P., Johnson, S., Joannopoulos, J., Ippen, E., and Smith, H., "A three-dimensional optical photonic crystal with designed point defects," *Nature* **429**, 538–542 (2004).